Theoretical prediction of two-dimensional II-V compounds

Lucia G. Arellano Sartorius,[1,2] Takayuki Suga,[1] Taichi Hazama,[1]
Taichi Takashima,[1] Miguel Cruz-Irisson,[2] and Jun Nakamura[1,*]

[1] *Department of Engineering Science, The University of Electro-Communications (UEC Tokyo), 1-5-1 Chofugaoka, Chofu, Tokyo 182-8585, Japan*

[2] *Instituto Politécnico Nacional, ESIME-Culhuacán, Av. Santa Ana 1000, C.P. 04440, Ciudad de México, México*

(Dated: December 9, 2022)

Graphene has attracted significant attention as a pioneer of two-dimensional zero gap semiconductors, but development of new two-dimensional materials with a finite band gap has been actively pursued. In this study, the structural stability of double bilayers (DBs) of group II-V compounds (II=Be, Zn, and Cd; V=P, As, and Sb) has been systematically investigated using first-principles calculations based on the density functional theory. The thermodynamical calculations have confirmed that BeP, BeAs, ZnP, and ZnAs can be produced through exothermic reactions from their constituent bulk systems. It has also been confirmed that all the compounds have the phonon dynamical stabilities. Only CdP and CdAs have been found to have an AB-stacked DB structure with the 3-fold symmetry, while the other compounds have AB'-stacked ones with broken symmetry. The difference in atomic radii between group II and group V results in the so-called size effect, which determines the stacking pattern. The structural stability of II-V DB thin films is explained by analogy with the surface structural stability of compound semiconductors: The change in an atomic arrangement in the DB structure alters the electronegativity of the surface orbitals of the II-V thin film, which does not result in any unsaturated bonds, *i.e.*, no metallic bands across the Fermi level appear. The various DB II-V compounds proposed in this study will join the ranks of atomic-level 2D semiconductor materials.

Keywords: 2D materials, double bilayers, semiconductors, density functional theory

I. INTRODUCTION

Since the discovery of graphene, research to develop new two-dimentsional (2D) materials has been vigorously pursued, attaining new properties, designing new devices, and using those in different applications like sensors [1], energy storage [2], transistors [3], spintronics [4], photocatalysis [5], hydrogen production [6], catalysis [7], and supercapacitors [8]. In recent years, not only graphene, but also various 2D materials have been investigated but which, unlike graphene, prefer to form the corrugated aromatic stage like borophene [9], silicene, germanene, plumbene, and stanene [10, 11]. Also various 2D compounds have been revisited such as hexagonal boron nitride [12–16], transition metal dichalcogenides (TMDs) [17–19], metal-organic frameworks [20], MX_2 [21], MXenes [22], Xenes [23], and TiO_2 ultra-thin films [24].

Searching for 2D allotropes of IV-IV and III-V binary compound semiconductors has also been pursued intensively. For example, Sahin *et al.* evaluated the structural stability of 2D thin films of various IV-IV and III-V binary compounds using first-principles calculations. They showed that atomic-level 2D structures could exist stably in various IV-IV and III-V combinations, such as SiC and GaN [25]. Later, they also showed that GaN monolayers form three-dimensional (3D) structures via van der Waals interaction [26]. Experimentally, AlN [27] and GaN [28] were identified on the Ag(111) and SiC(0001) surfaces, respectively. It was also reported that the electronic and optical properties of binary compounds could be controlled by biaxial strain [29]. The applications of layered structures of IV-IV compounds to hydrogen storage materials [30–36] and battery electrodes [37–39] have also attracted attention. Recently, another class of 2D structures in typical compound semiconductors was proposed using first-principles calculations [40]. This class of compounds with a double-layered honeycomb (DLHC) structure consists of typical III-V, II-VI, and I-VII semiconductors. Very recently, it was reported that the 2D AlSb thin film with the DLHC structure could be grown on a SiC(0001) surface through van der Waals epitaxy [41].

Many 2D-isolated compound thin films, such as III-V and II-VI compounds, often have an even number of valence electrons per chemical unit. This is because an even number of electrons in a system can form a covalent bond of a complete pair of electrons. Group III monochalcogenides such as GaSe, however, have long been known as 2D compounds [42, 43] in which the smallest chemical unit has an odd number of valence electrons. III-VI compounds

* jun.nakamura@uec.ac.jp

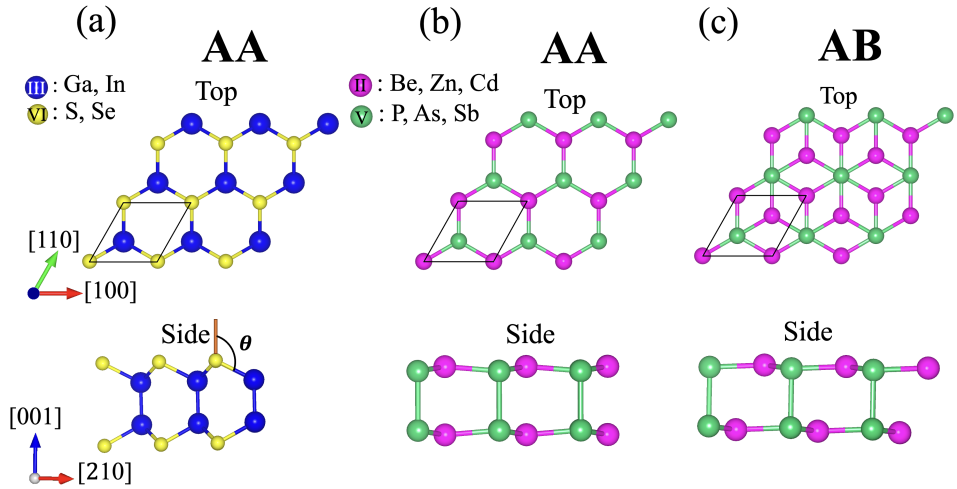

FIG. 1. Top and side views of initial structures of DB-stacked III-VI and II-V compounds. (a) AA-stacking for III-VI compounds, (b) AA-stacking and (c) AB-stacking for II-V compounds. Parallel quadrilaterals indicate primitive cells. Crystal orientation is shown in triaxial representation, assuming a hexagonal crystal structure.

are semiconductor and thermodynamically stable despite the odd number of valence electrons per chemical unit because III-VI compounds have a double bilayer (DB) structure, resulting in the disappearance of dangling bonds on the surface. Such a semiconducting nature of the III-VI DB structure can be understood based on the electron counting (EC) [44] and the bond orbital (BO) [45–47] models often used in discussions of the stability of compound semiconductor surfaces, as we will verify in this paper. Given that analogy, it is not surprising to predict that thin film structures nearly identical to the III-VI DB structure will also exist in II-V compounds based on the EC model. Indeed, it was reported that a 2D layered Zintl phase of ZnSb was successfully fabricated by treating non-layered ZnSb crystals with Li [48]. In addition, the hydrogenated ZnSb monolayer was expected to be promising candidate for applications in electronics and opto-electronics [49]. The DB ZnSb thin film [48, 50], which is the building block of the layered ZnSb, and another II-V combination, the DB BeP [51], were confirmed to have a finite band gap, showing a semiconducting nature using theoretical calculations. DB CdAs have also recently been theoretically confirmed to be stable [52]. However, no common insight into the stabilization mechanism of ultra-thin films of II-V compounds has been obtained yet. In this paper, based on the EC and the BO models, we provide a mechanism for the structural stabilization of II(Be, Zn, Cd)-V(P, As, Sb) and III-VI (GaSe, GaS, and InSe) ultra-thin films with DB structures through a systematic characterization of their atomic arrangements and electronic structures using first-principles calculations within the density functional theory (DFT). All the DB II-V structures examined in this study were found to be stable, and their optimized stacking structures can be classified into two types of DBs, AB and AB'. This difference in stacking fashion yields a difference in the symmetry of the system. As a result, it was shown that the AB structure with higher symmetry becomes a Dirac semimetal, and the gap is opened at the Dirac cone as a consequence of the spin-orbit coupling (SOC), while the AB' structure has a normal semiconducting nature based on the EC and BO models.

II. CALCULATION MODELS AND METHOD

Figure 1 shows examples of the initial structure for the DB compounds. It has been known that the DB III-VI compounds have the AA stacking [53, 54] as shown in Fig. 1(a). This structure is very similar to the DB structure of the so-called Wurtzite(0001), but the stacking order is different. As a result, the DB Wurtzite(0001) structure has C_{3v} symmetry, while the DB III-VI possesses higher symmetry, D_{3h}. For II-V compounds, we considered the AA-stacking structure shown in Fig. 1(b), which is similar to III-VI compounds, and the AB-stacking (zinc-blende-like) structure shown in Fig. 1(c), known as an isomer of the AA-stacking structure [55], as the initial structures. In order to identify the veritable most stable structure, we tried various initial configurations in which group II and V atoms are bonded with each other and also models in which group II atoms are bonded between DBs as the initial structure. All the initial atomic configurations are shown in Figure S1 in the Supplemental Material.

We investigated the structural stability of DB III-VI and II-V compounds using first-principles calculations within the DFT [56] using the Vienna *ab initio* simulation package (VASP) code [57, 58]. The generalized gradient approx-

imation (GGA), PBE [59], was adopted as the exchange-correlation functional. It was reported for DB CdAs that the SOC has an intrinsically significant effect on the electronic structure [52]; thus, the SOC was also considered. It is generally known that the GGA level calculations underestimate the band gap. In some cases, materials that are supposed to be semiconductors may be predicted to have metallic electronic states. Therefore, we adopted the HSE06 hybrid functional [60] in the present study to calculate the energy bands when the PBE level calculations resulted in metallic electronic states. The cutoff energy of plane wave expansion was taken to be 550 eV. The increase in cutoff energy up to 700 eV had little effect on the atomic arrangement or electronic structure discussed in this study. The convergence criterion of self-consistent calculations was 10^{-6} eV for total energies. Fermi-level smearing was not taken in this study. The projector augmented wave method was used [61, 62]. $(18 \times 18 \times 1)$ k points were used for the integration in $\boldsymbol{k}$ space in the Brillouin zone (BZ) for the primitive cell. The atomic position was optimized such that the force acting on each atom became less than 1.0×10^{-3} eV/Å. Since the atomic arrangement of 2D materials can be dominated by van der Waals (vdW) interactions, we also carried out the calculations using the vdW correction [63]. However, it was confirmed that the atomic arrangement and the electronic structure were almost unchanged. Thus, the vdW interaction has no effect if the proposed materials are in the isolated DB structure. After all, the vdW interaction was not considered in this study. The phonon dispersions were calculated with a supercell approach, as implemented in the Phonopy code [64]. We performed phonon calculations using cells that guaranteed sufficient accuracy; the supercells consisting of the $(5 \times 5 \times 1)$ primitive units for ZnP, ZnAs, ZnSb, CdP, CdAs, CdSb, BeSb, and the $(3 \times 3 \times 1)$ unit for BeAs, where the corresponding q-point grid was set to $(3 \times 3 \times 1)$. As for BeP, the $(7 \times 7 \times 1)$ supercell and the $(1 \times 1 \times 1)$ q-point grid.

III. RESULTS AND DISCUSSION

The stability of the surface structures of III-V and II-VI compound semiconductors has long been discussed using the EC model [44] and the BO model [45–47] based on the orbital electronegativity [65]. The EC model discusses the stabilization mechanism of the surface as follows: on the surface, dangling bonds of group III (II) atoms become empty and dangling bonds of group V (VI) atoms become lone pairs, forming a semiconducting electronic state. The charge transfer mechanism is explained by the change in the orbital electronegativity of the dangling bonds depending on the back-bond angle of the surface atoms with respect to the dangling bonds [46, 47]. In this study, we apply these models to the DB III-VI and II-V compounds to examine their structural stabilities.

A. Double bilayers compounds of group III-VI

The structure and electronic structure of DB GaSe are well understood through previous studies [66–70]. In this section, we first show that our calculations can reproduce the previous results. We then show that the structural stability of DB GaSe can be intuitively revisited in terms of chemical bonding theory through the EC and BO models and the electron localization function (ELF) [71, 72] which shows a measure of the probability of electron pairs. We consider GaSe as a typical example of a III-VI DB and try to understand its structural stability based on the BO model. In the DB GaSe, the Se layer is located at the top and bottom surfaces, and the Ga layer forms the inner layer. Each Se atom has a surface orbital in the surface vacuum direction. In the DB structure, all atoms are basically located in the so-called tetrahedral position and have sp^3-like bonds. In Fig. 1 (a) are shown the back-bond angle of the surface orbital of the topmost surface atom (θ) the value for GaSe was 118.1°, which is consistent with the previous calculations [70] and is larger than the bond angle of the ideal sp^3-hybridized orbital, 109.5°.

The BO model indicates that the larger the back-bond angle of the surface orbital, the larger its s-character and, consequently, the larger the electronegativity of the surface orbital. Thus, the orbital electronegativity of the surface orbital of the Se atom is larger than that of the ideal sp^3 orbital. In the BO model, it is assumed that all chemical bonds between atoms form sp^3 covalent bonds. If the bonds between Ga-Ga layers are covalent, each Ga atom provides one valence electron to the Ga-Ga bonds between the layers. Since the Se atom has 6 valence electrons, it would provide 6/4 electrons to each of the four hands around it. If 2/3 and 6/4 electrons by Ga and Se are supplied to the bond between the surface Ga-Se atoms, respectively, there will be (2 + 1/6) electrons, resulting in excess of 1/6 electrons when the covalent bond is formed. Since the orbital electronegativity of the surface orbitals of the topmost Se atom is larger than that of the ideal sp^3 bond and attracts electrons, the excess $(1/6) \times 3$ electrons from the three Ga-Se bonds transfer to the surface orbitals. As a result, there are $(6/4 + 1/6 \times 3) = 2$ electrons in the Se surface orbitals, *i.e.*, a lone pair is formed.

Therefore, there is no surface dangling bond in III-VI ultra-thin films, and the electronic state becomes semiconducting and stabilized. Indeed, as shown in Fig. 2 (a), the DB GaSe has a finite indirect band gap, as reported elsewhere [69]. Figure 2(b) shows the spatial distribution of the ELF for DB GaSe. As clearly shown in this figure,

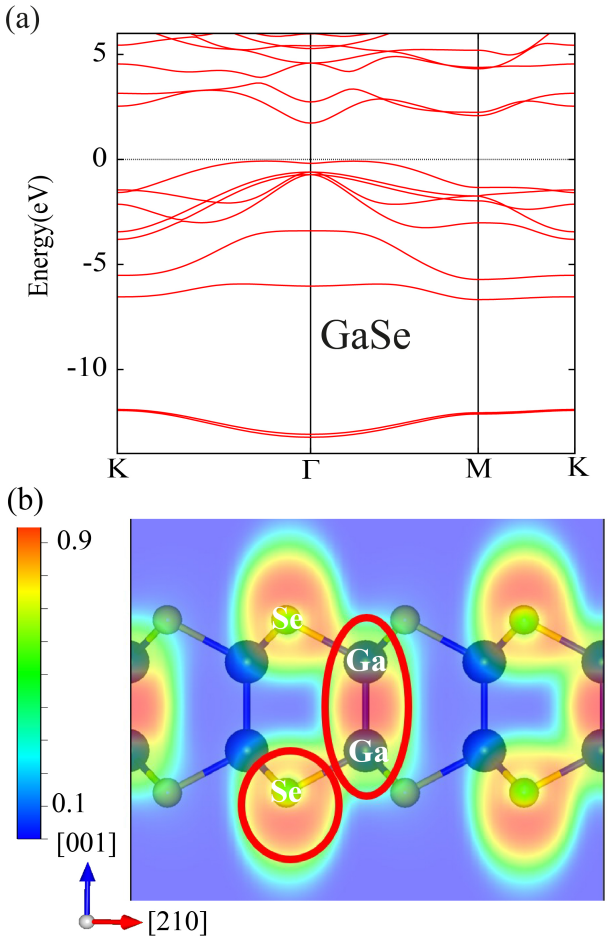

FIG. 2. (a) Band structure of the DB GaSe compound. The dashed line shows the top of the valence band. (b) Electron localization functions for the GaSe in the cross section including the Se-Ga-Ga-Se bonding network.

high ELF values are observed at the positions just above the surface Se atoms and the Ga-Ga interatomic positions between the DBs, definitely indicating the covalent bond (red ellipse) and the lone pair (red circle) formations. The band diagrams and ELFs for the other compounds of the group III-VI, GaS and InS, are also shown in Figs. S3 and S4 in the Supplemental Material. It is clear from these results that in the DB III-VI compounds, the semiconducting electron configuration realizes as qualitatively predicted by the BO model.

Therefore, we can conclude that the band gap opening, or semiconducting nature, is the origin of the structural stabilization in DB III-VI compounds, as expected from the EC and BO models.

B. Double bilayers compounds of group II-V

In this study, we evaluate the possibility of the existence of the DB structure of group II-V compounds as an analogy to group III-VI compounds. In the DB structure of III-VI compounds, the origin of stabilization is that the surface orbitals of the topmost group VI atoms form a lone pair, and the electronic state becomes a closed shell structure. Therefore, the II-V DB is expected to stabilize when the surface orbitals of not group V but group II atoms are empty. Based on the BO model, two valence electrons of the surface group II atom are distributed to 4 sp^3 bonds; thus, the surface orbital has two-quarters electrons if all atoms are covalently bonded with each other. If the bond between V-V group is covalent between the layers, the group V atom of each BL provides one electron for each of its bonds. The remaining four electrons from the group V atom are distributed to the three neighboring bonds in the BL plane by 3/4 electrons each. The group II atom must supply 2/3 electrons to each of the three bonds in the BL plane in order for the bonds to form the covalent bond. As a result, the electrons of the surface orbital should be transferred

TABLE I. Stacking fashion (SF), lattice constant (a), lattice angle; angle between the primitive lattice vector in the 2D plane (α), stacking energy ($E_{\rm s}$), formation energy ($\Delta H_{\rm f}$), cohesion energy ($\Delta H_{\rm coh}$), and band gap with the PBE functional ($E_{\rm g}^{\rm PBE}$) and with the HSE one ($E_{\rm g}^{\rm HSE}$).

	SF	a (Å)	α (°)	$E_{\rm s}$ (eV/atom)	$\Delta H_{\rm f}$ (meV/atom)	$\Delta H_{\rm coh}$ (eV/atom)	$E_{\rm g}^{\rm PBE}$ (eV)	$E_{\rm g}^{\rm HSE}$ (eV)
BeP	AB'	3.70	60.08	-0.67	+283.8	3.77	1.72	2.61
BeAs	AB'	3.87	59.69	-0.56	+46.21	3.37	1.27	2.08
BeSb	AB'	4.25	56.30	-0.49	-523.3	2.96	0.0	0.36
ZnP	AB'	4.07	60.60	-0.59	+121.4	2.37	1.03	1.86
ZnAs	AB'	4.26	60.28	-0.47	+90.9	2.08	0.80	1.56
ZnSb	AB'	4.61	59.73	-0.43	-114.8	1.85	0.91	1.62
CdP	AB	4.44	60.00	-0.64	-138.7	2.06	metallic	metallic
CdAs	AB	4.61	60.00	-0.51	-27.8	1.84	metallic	metallic
CdSb	AB'	4.92	60.31	-0.46	-94.2	1.68	0.29	0.73

to neighboring bonds for the surface orbitals of group II atoms to become empty, leading to no dangling bond at the surface. This charge transfer should be achieved by the reduction of the buckling angle of the surface, that is, the smaller orbital electronegativity of the surface orbital of each group II atom. Therefore, a relatively planar bilayer (BL) structure is required. Furthermore, for group II atoms to form empty surface orbitals, a network formation of II-V-V-II perpendicular to the surface is required, *i.e.*, group V atoms must form covalent bonds between DBs.

First, stacking configurations were optimized for several stacked-structure models as described in the Models section, and their stabilities were evaluated in terms of stacking energy, ($E_{\rm s}$), defined by the following equation:

$$E_{\rm s} = \frac{E_{\rm DB} - (E_{\rm BL} \times 2)}{4}, \tag{1}$$

where $E_{\rm DB}$ and $E_{\rm BL}$ are the total energies of DB II-V and single BL II-V per primitive cell. A negative value of $E_{\rm s}$ means that the compound is stabilized by the stacking of BL rather than the free-standing BL. The calculated values of $E_{\rm s}$ are listed in Table I. All DB II-V compounds considered in this study have attractive interactions between BLs. What has to be noticed is that two types of stacking structures, AB and AB', were found depending on the combination of group II and group V atoms. The AB' configuration was the most stable for BeP, BeAs, BeSb, ZnP, ZnAs, ZnSb, and CdSb, while AB for CdP and CdAs. In the AB' configuration, each BL is displaced slightly from the just AB stacking along the [210] direction, as shown in Fig. 3. In the AB stacking system, the BLs form bonds between group V atoms, whereas in the AB' stacking system, the nearest atoms between the DBs are not always pairs of group V atoms due to the displacement between the BLs (see Figs. S5, S6, and S7 of the Supplemental Material). More noteworthy here is the fact that the symmetry of the system in the AB' stacking is broken: The AB stacking system has exact 3-fold symmetry, C_{3v}, whereas the AB' one only has a vertical mirror plane parallel to the [210] direction, leading to a deviation of the lattice angle, α, from 60°, as shown in Table I.

The thermodynamical stability of the system was evaluated using the formation energy per atom, $\Delta H_{\rm f}$, of II-V DB compounds defined as follows:

$$\Delta H_{\rm f} = E_{\rm II\text{-}bulk} + E_{\rm V\text{-}bulk} - E_{\rm II\text{-}V}, \tag{2}$$

where $E_{\rm II(V)\text{-}bulk}$ is the total energy of group II(V) bulk per atom and $E_{\rm II\text{-}V}$ corresponds to a quarter of the total energy per (1×1) unit cell of DB II-V. The crystal structures of the group II and group V bulk, employed for the calculation of the formation energy, are listed in Table S1 in the Supplemental Material. If $\Delta H_{\rm f}$ is positive (negative), then the reaction becomes exothermic (endothermic). Figure 4 shows the calculated values of $\Delta H_{\rm f}$ for each group II series. It has been shown that BeP, BeAs, ZnP, and ZnAs have positive $\Delta H_{\rm f}$ values, indicating that the reaction proceeds exothermically when metal elements of group II and V are used as starting materials. The cohesive energy per atom, $\Delta H_{\rm coh}$, of II-V DB compounds, defined as follows, was also evaluated:

$$\Delta H_{\rm coh} = E_{\rm II\text{-}atom} + E_{\rm V\text{-}atom} - E_{\rm II\text{-}V}, \tag{3}$$

where $E_{\rm II(V)\text{-}atom}$ is the total energies of isolated group II(V) atom and $E_{\rm II\text{-}V}$ corresponds to a quarter of the total energy per (1×1) unit cell of DB II-V. The calculated values of $\Delta H_{\rm coh}$ are listed in Table I. The result for the BeP DB compound was 3.77 eV/atom, which agrees well with the result reported by Meng *et al.* [51]. Other results of lattice parameters and bond lengths for DB BeP reproduced those by Meng *et al.* [51].

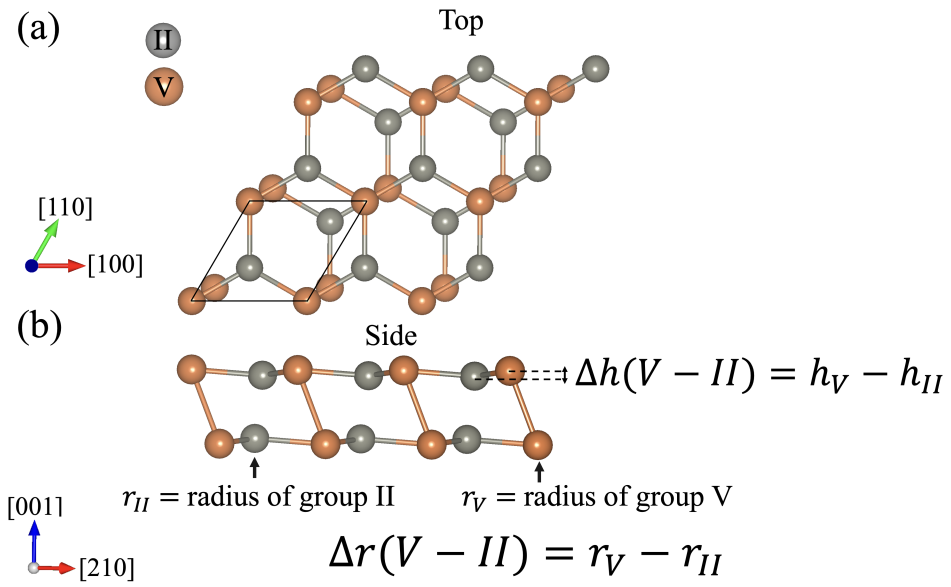

FIG. 3. (a) Top and (b) side views of the AB' configuration.

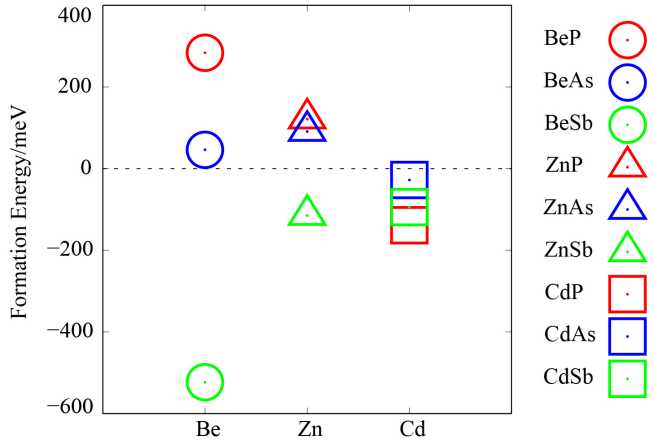

FIG. 4. Formation energy, ΔH_{f}, of II-V DB compounds for each group II series. Red, blue, and green indicate that the group V elements are P, As, and Sb, respectively.

We calculated the electronic band structures for the optimized structures. The results within the PBE functional show that the group II-V DB compounds exhibit metallic or semiconductor behaviour depending on their combinations. As shown in Table I, the BeP, BeAs, ZnP, ZnAs, ZnSb, and CdSb DBs have finite energy gap, showing the semiconducting nature, whereas the CdP and CdAs DBs are metallic and BeSb becomes a zero (finite) gap semiconductor with PBE (HSE06) functional. Figures 5(a) and 5(c) show the electronic band dispersions for ZnAs and CdAs DBs, as examples. The band structure of other compounds are shown in Figs. S8-S10 in the Supplemental Material. Viewed in this light, we can conclude that all DB II-Vs except for CdP and CdAs have no metallic bands, *i.e.*, the EC and the BO models are satisfied. Furthermore, it has been revealed that the AB-stacked DB with a higher symmetry has metallic bands crossing the Fermi level, while the AB'-stacked one becomes a semiconductor.

In order to evaluate the chemical bonding fashion, we calculated the ELF for the DB II-V. Figure 5(b) shows the spatial distribution of ELF for the ZnAs DB compound as an example. The ELF values are larger in the vicinity of the As atoms, indicating that covalent bonds are formed between the As atoms in each BL. However, due to the more planar nature of the BL structure, strong covalent bonds are not formed between BLs, because not sp^3 but p_z-like orbitals will mainly contribute to the bonding between BLs. In addition to that, there would be ionic bonds between As and Zn, which are closer together due to the in-plane shift between BLs. As a result, ionic bonds between BLs also contribute to the stability of the system as well as covalent bonds. Such features were also observed in other II-V

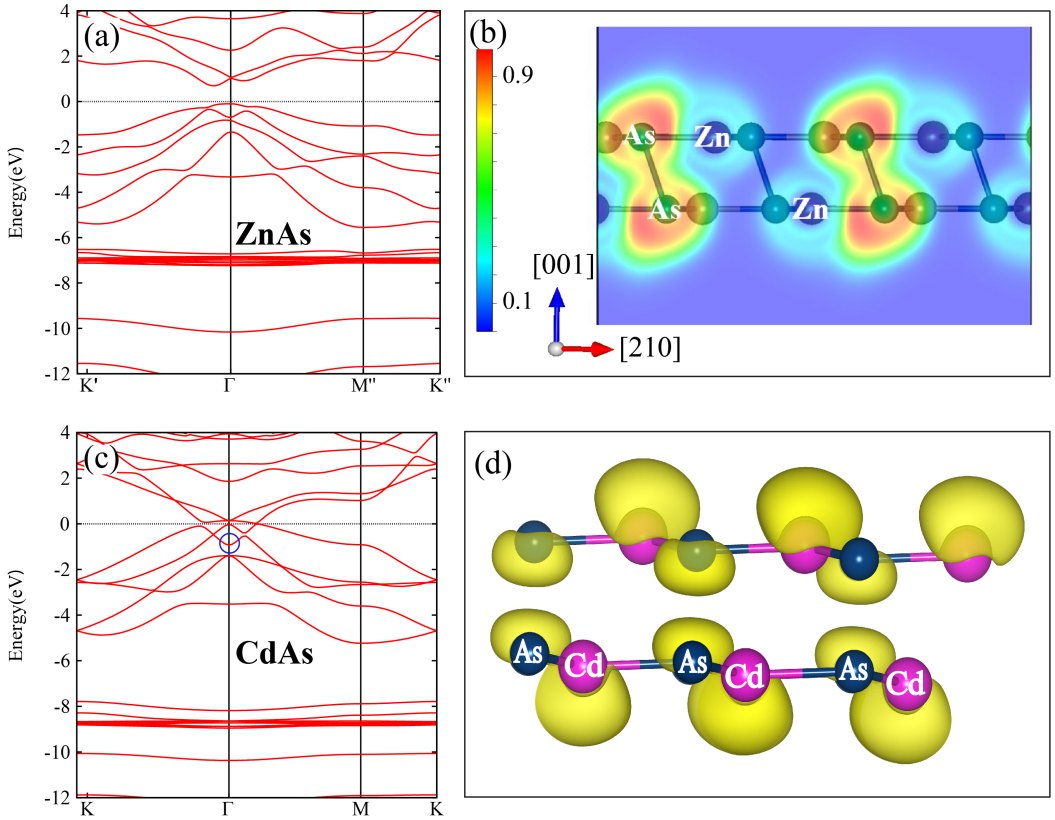

FIG. 5. (a) Band structure and (b) ELF of DB ZnAs. (c) Band structure and (d) the isosurface of the probability density for DB CdAs at the Γ point for the metallic band marked with a circle in Fig. 5(c). The top of the valence band and the Fermi energy were set to 0 eV for DB ZnAs and DB CdAs, respectively.

combinations than ZnAs, as shown in Figs. S15-S17 in the Supplemental Material.

We discuss the atomic arrangement in more detail. Under the EC model, the electron configuration of group V atoms must be in a closed shell structure, and the group II surface orbitals must become empty for the system to be stable. To be achieved this situation, each BL must be nearly flat based on the BO model. On the other hand, if the BLs were completely flattened, the BLs would be weakly coupled between p_z orbitals instead of sp^3. Therefore, the stability of the system must be determined by a trade-off between the charge-transfer mechanism of the system based on the BO model and the degree of bond formation between BLs. The flatness of each BL was evaluated in terms of the degree of buckling in the BL, *i.e.*, the difference in coordinates between group II and V atoms on the [001] axis, Δh(V-II), defined in Fig. 3 (b). Thus, if the sign of Δh(V-II) is positive (negative), then the group V (II) atom locates at the topmost surface of DB. It has been confirmed that CdP, CdAs, CdSb, and ZnP, have negative Δh(V-II) values, meaning that group II atoms appear at the topmost surface of the DB structure. Furthermore, it has been found that the magnitude of buckling is strongly related to the difference in atomic radius [73] of group II and V atoms, Δr(V-II). Figure 6 shows the Δh(V-II) as a function of Δr(V-II). We can confirm the strong correlation (0.99) between them. Furthermore, it has been found that if Δh(V-II) is positive, then Δr(V-II) is also positive, and vice versa, *i.e.*, atoms with larger atomic radius prefer to locate at the topmost surface. Such results remind us of the so-called size effect, well-known at an atomic scale, for example, for surfactants on semiconductor surfaces or surface segregation [74, 75]. Strong correlations of the surface buckling with the difference in atomic radius between group II and group V were also confirmed with covalent, ionic, ionic crystal, and metal radii, as shown in Figs. S18 and S19 in the Supplemental Material. Such a size effect would inhibit the formation of the flat surface structure predicted by the BO model. When group V atoms are too large, such as in BeSb, the system becomes relatively unstable because the group V atom locates on the topmost surface, and the bonds between BLs are formed at Sb-Be rather than Sb-Sb between BLs. On the other hand, even when group II atoms are too large, such as in CdP and CdAs, group II atoms locate on the topmost surface and the electronegativity of their surface orbitals becomes large, which work against the full establishment of the BO model. In fact, CdP and CdAs with the AB stacking structure are metallic, as shown in Table I. As can be seen in Fig. 5(c), the band that would be the conduction band if the system

were semiconductor shifts below the Fermi level. Indeed, this band has an anti-bonding character attributed to the Cd atom at the Γ point, as shown in Fig. 5(d). The large back-bond angle leads to a large electronegativity of the surface orbital of Cd, being partial occupation of this state. Based on the BO and the EC models, the group V atoms in DB II-V compounds should be fully occupied and the surface orbitals of the group II atoms should be unoccupied. Therefore, the flatter the BL structure, the more likely the BO and the EC models become valid. In this case, the bonding between BLs requires covalent bonding between group V atoms. On the contrary, if the BL structure is completely flat, the inter-BL must bond between p_z orbitals, which is not necessarily energetically favorable. Thus, a more sp^3-like orbital component than p_z is required in the interlayer bonding. As a result, BeP and ZnP, where the atomic radii of group V and II atoms are slightly different, become relatively stable compared with the nearly-flat compounds like ZnAs and CdSb. In other words, in DB II-V compounds, the optimal combination of group II and V elements and the most stable structure are determined by the trade-off between the requirements of the simplified BO and EC models for the bonding fashion and the size effect due to the difference in atomic radius between group II and group V atoms. As a matter of fact, the stacking energy of CdP (-0.64 eV/atom) and CdAs (-0.51 eV/atom) is greater than that of BeSb (-0.49 eV/atom). Therefore, to obtain a more significant gain in binding energy between these V-V atoms, CdP and CdAs prefer AB stacking. Such a relationship between the flatness of each BL and the BL-BL binding energy can also be confirmed in terms of the stacking energy shown Table I. For example, in the Be series, Δh(V-II) becomes smaller and flatness increases in the order of BeSb, BeAs, and BeP, while the stacking energy decreases in this order. This trend is not clear in the Zn series because Δh(V-II) is relatively tiny, but it is clearly observed in the Cd series. Finally, it is worth mentioning that AB-stacking is the most stable for CdP and CdAs with large atomic radius differences, while AB'-stacking is maintained for BeP with similarly large atomic radius differences. This is due to the difference in whether the bonds between DBs are II-II or V-V. In DB II-V, group V atoms are anion-like and group II atoms are cation-like. Therefore, the bonds between the more electron-rich group V atoms should be stronger than those between group II atoms.

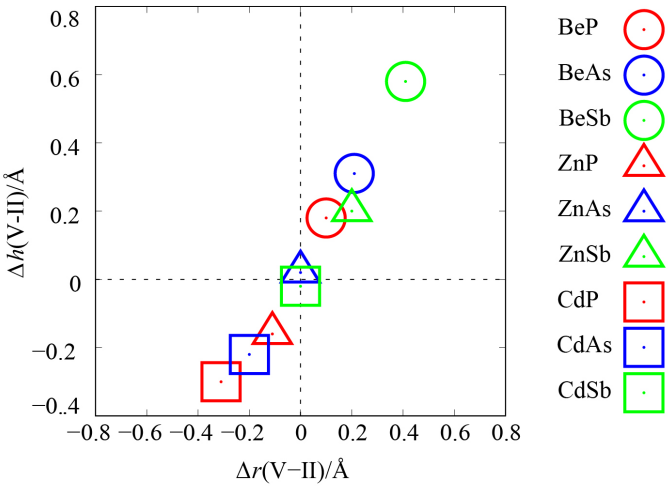

FIG. 6. Relationship between the roughness of BL, Δh(V-II), and the difference in atomic radius, Δr(V-II), of DB group II-V compounds (see text). Group V elements P, As, and Sb are indicated by red, blue, and green colors, respectively. Circle, triangle, and square identify the group II atoms as Be, Zn, and Cd, respectively.

Here, the metallic nature of DB CdP and DB CdAs is worth a mention. As shown in Figs. 5(c) and 5(d), the valence and conduction bands of DB CdAs crosses with each other without opening a gap, indicating the manifestation of topological properties [76]. The same situation was also confirmed in DB CdP shown in Fig. S10(a). Recently, it was proposed that the DB CdAs is in a class of nontrivial topological material; DB CdAs is a semimetal with six equivalent Dirac cones on the paths of Γ-M, and these cones are protected by vertical mirror symmetries [52]. Then, we re-run the calculations for all the combinations to evaluate the effect of SOC. We confirmed that for the systems that are semiconductors when ignoring SOC, the atomic arrangements and energy bands hardly change even when SOC is taken into account. As a result, the value of the band gap does not change with SOC for the AB'-stacking systems. However, not only CdAs but also AB-stacked CdP were confirmed to generate a slight gap at the Dirac point along the Γ-M direction when SOC is considered, as shown in Fig. S14. As a result, the DB CdAs with the AB stacking should no longer be considered a metal but a system with a bandgap of about 30 meV. On the other hand, the DB CdP with the AB stacking remained metallic even when considering SOC. Furthermore, looking at the band structure of DB CdSb without SOC shown in Fig. S10(C), the degeneracy at the Dirac point appears to be lifted.

The Dirac point of CdAs or CdP is protected by three equivalent vertical mirrors within the C_{3v} symmetry. From this point of view, one may say that the symmetry reduction caused the band gap opening in the CdP. Such a change in symmetry is directly associated with the size effect at the atomic level. Thus, DB CdP is also a promising candidate for a new topological material. Nevertheless, there is room for further investigation beyond the discussion envisioned in this paper.

Finally, we examined the phonon stability of each compound. Figures S21(c) and S21(a) in the Supplemental Material show the phonon dispersion relations for ZnSb, which has been experimentally confirmed to have a layered structure, and for BeP, which has a highest formation energy. The result for metallic CdP is also shown in Fig. S21(a). In the limit of $q = 0$, these DB compounds exhibit the linear LA and TA branches, and also the quadratic ZA branch related to the vibration perpendicular to the surface that is characteristic of ordinary 2D materials [25, 77]. Furthermore, we can also confirm that no imaginary phonons appear. Therefore, we can conclude that all the DB II-V compounds analyzed in this study have good dynamical stabilities due to the absence of imaginary frequencies. The phonon bands of all the compounds can be found in Figs. S20-S22 in the Supplemental Material.

IV. CONCLUSIONS

This study systematically discussed the structural stability and electronic structure of ultra-thin group II-V (II:Be, Zn, and Cd, V:P, As, and Sb) compound films. We have first taken the DB III-VI compounds as examples to illustrate the origin of its structural stabilization using the EC and BO models. The EC model has attributed the structural stability of the DB III-VI compounds to the strong covalent bonds and the lone pairs at the surface instead of a dangling bond. The BO model has consistently explained the charge transfer between surface atoms based on the orbital-electronegativity predicted from the optimized structure.

It has been revealed that II-V compounds with DB structures like 2D III-V and III-VI films are energetically stable. In the DB II-V compounds, we have found two types of stacking configuration, AB and AB'. DB CdP and DB CdAs compounds having the AB-stacked structure become metallic when SOC is ignored. On the other hand, DB BeP, BeAs, BeSb, ZnP, ZnAs, ZnSb, and CdSb compounds have AB'-stacked structures. The AB'-stacking results in a lower symmetry (σ_v) compared with the AB-one (C_{3v}). The DB II-V with an AB' stacking results in the fully occupied valence and empty conduction bands. The semiconducting nature of the system is considered to be one of the origin of the stability in DB II-V as well as DB III-VI. As a result, it has been revealed that the AB structure with higher symmetry becomes a Dirac semimetal, and the gap is opened at the Dirac cone, while the AB' structure has a normal semiconducting nature as predicted from the EC and BO models. There are no imaginary phonon frequencies for all compounds explored. Thus, the phonon stability has also been confirmed. Unlike in the case of III-VI and III-V, in the case of II-V, the atomic species that constitute the surface side of the DB configuration depend on the combination of II and V, because the so-called size effect is prominently manifested; elements with larger atomic radius are located on the top surface. In addition, the larger the difference in the atomic radius, the larger the buckling angle of the surface, leading to the manifestation of the so-called size effect. It has been found that the system is electronically more stable when the difference in atomic radii between group II and V is relatively smaller, because, based on the BO model, the atomic arrangement must be flat in each BL in order for a surface orbital of group II atom to become empty. However, the flatter each BL becomes, the weaker the interaction between the DB planes becomes. On these grounds, the stability of the system is dominated by the balance of the covalent bond formation between DB planes and the size effect.

We have proposed novel 2D materials, DB II-V (BeP, BeAs, BeSb, ZnP, ZnAs, ZnSb, CdP, CdAs, and CdSb) compounds through the analysis of electronic and phonon properties. These materials would provide a new platform for 2D material families. In light of the experimental confirmation that intercalating Li into bulk ZnSb yields layered ZnSb structures [48], stacking structures of various group II-V DB are promising as alkali metal storage materials or electrode materials for ion batteries.

[1] R. Chaurasiya and A. Dixit, Ultrahigh sensitivity with excellent recovery time for NH_3 and NO_2 in pristine and defect mediated Janus WSSe monolayers, Physical Chemistry Chemical Physics **22**, 13903 (2020).

[2] M. K. Aslam, T. S. AlGarni, M. S. Javed, S. S. A. Shah, S. Hussain, and M. Xu, 2D MXene materials for sodium ion batteries: a review on energy storage, Journal of Energy Storage **37**, 102478 (2021).

[3] S.-K. Su, C.-P. Chuu, M.-Y. Li, C.-C. Cheng, H.-S. P. Wong, and L.-J. Li, Layered semiconducting 2D materials for future transistor applications, Small Structures **2**, 2000103 (2021).

[4] W. Chen, Y. Qu, L. Yao, X. Hou, X. Shi, and H. Pan, Electronic, magnetic, catalytic, and electrochemical properties of two-dimensional janus transition metal chalcogenides, Journal of Materials Chemistry A **6**, 8021 (2018).

[5] W. Chen, X. Hou, X. Shi, and H. Pan, Two-dimensional janus transition metal oxides and chalcogenides: multifunctional properties for photocatalysts, electronics, and energy conversion, ACS Applied Materials & Interfaces **10**, 35289 (2018).

[6] X. Li, J. Zhang, S. Zhang, S. Xu, X. Wu, J. Chang, and Z. He, Hexagonal boron nitride composite photocatalysts for hydrogen production, Journal of Alloys and Compounds **864**, 158153 (2021).

[7] F. R. Fan, R. Wang, H. Zhang, and W. Wu, Emerging beyond-graphene elemental 2D materials for energy and catalysis applications, Chemical Society Reviews **50**, 10983 (2021).

[8] G. Murali, J. Rawal, J. K. R. Modigunta, Y. H. Park, J.-H. Lee, S.-Y. Lee, S.-J. Park, and I. In, A review on MXenes: new-generation 2D materials for supercapacitors, Sustainable Energy & Fuels **5**, 5672 (2021).

[9] P. Ranjan, J. M. Lee, P. Kumar, and A. Vinu, Borophene: New sensation in flatland, Advanced Materials **32**, 2000531 (2020).

[10] K. Takeda and K. Shiraishi, Theoretical possibility of stage corrugation in Si and Ge analogs of graphite, Physical Review B **50**, 14916 (1994).

[11] J. Yuhara and G. Le Lay, Beyond silicene: synthesis of germanene, stanene and plumbene, Japanese Journal of Applied Physics **59**, SN0801 (2020).

[12] Y. Lin, T. V. Williams, and J. W. Connell, Soluble, exfoliated hexagonal boron nitride nanosheets, The Journal of Physical Chemistry Letters **1**, 277 (2010).

[13] K. Zhang, Y. Feng, F. Wang, Z. Yang, and J. Wang, Two dimensional hexagonal boron nitride (2D-hBN): synthesis, properties and applications, Journal of Materials Chemistry C **5**, 11992 (2017).

[14] A. García-Miranda Ferrari, S. J. Rowley-Neale, and C. E. Banks, Recent advances in 2D hexagonal boron nitride (2D-hBN) applied as the basis of electrochemical sensing platforms, Analytical and Bioanalytical Chemistry **413**, 663 (2021).

[15] L. H. Li and Y. Chen, Atomically thin boron nitride: unique properties and applications, Advanced Functional Materials **26**, 2594 (2016).

[16] R. C. Andrew, R. E. Mapasha, A. M. Ukpong, and N. Chetty, Mechanical properties of graphene and boronitrene, Physical Review B **85**, 125428 (2012).

[17] C. Tan, X. Qi, X. Huang, J. Yang, B. Zheng, Z. An, R. Chen, J. Wei, B. Z. Tang, W. Huang, *et al.*, Single-layer transition metal dichalcogenide nanosheet-assisted assembly of aggregation-induced emission molecules to form organic nanosheets with enhanced fluorescence, Advanced Materials **26**, 1735 (2014).

[18] H.-P. Komsa and A. V. Krasheninnikov, Two-dimensional transition metal dichalcogenide alloys: stability and electronic properties, The Journal of Physical Chemistry Letters **3**, 3652 (2012).

[19] D. Geng and H. Y. Yang, Recent advances in growth of novel 2D materials: beyond graphene and transition metal dichalcogenides, Advanced Materials **30**, 1800865 (2018).

[20] T. Rodenas, I. Luz, G. Prieto, B. Seoane, H. Miro, A. Corma, F. Kapteijn, F. X. Llabres i Xamena, and J. Gascon, Metal–organic framework nanosheets in polymer composite materials for gas separation, Nature Materials **14**, 48 (2015).

[21] M. Kar, R. Sarkar, S. Pal, and P. Sarkar, Tunable electronic structure of two-dimensional MoX_2 (X= S, Se)/SnS_2 van der Waals heterostructures, The Journal of Physical Chemistry C **124**, 21357 (2020).

[22] M. Naguib, V. N. Mochalin, M. W. Barsoum, and Y. Gogotsi, 25th anniversary article: MXenes: a new family of two-dimensional materials, Advanced Materials **26**, 992 (2014).

[23] A. Molle, J. Goldberger, M. Houssa, Y. Xu, S.-C. Zhang, and D. Akinwande, Buckled two-dimensional Xene sheets, Nature Materials **16**, 163 (2017).

[24] B. R. Bricchi, M. Sygletou, L. Ornago, G. Terraneo, F. Bisio, C. Mancarella, L. Stasi, F. Rusconi, E. Mogni, M. Ghidelli, *et al.*, Optical and electronic properties of transparent conducting Ta: TiO_2 thin and ultra-thin films: the effect of doping and thickness, Materials Advances **2**, 7064 (2021).

[25] H. Şahin, S. Cahangirov, M. Topsakal, E. Bekaroglu, E. Akturk, R. T. Senger, and S. Ciraci, Monolayer honeycomb structures of group-IV elements and III-V binary compounds: First-principles calculations, Physical Review B **80**, 155453 (2009).

[26] A. Onen, D. Kecik, E. Durgun, and S. Ciraci, Gan: From three-to two-dimensional single-layer crystal and its multilayer van der Waals solids, Physical Review B **93**, 085431 (2016).

[27] P. Tsipas, S. Kassavetis, D. Tsoutsou, E. Xenogiannopoulou, E. Golias, S. Giamini, C. Grazianetti, D. Chiappe, A. Molle, M. Fanciulli, *et al.*, Evidence for graphite-like hexagonal aln nanosheets epitaxially grown on single crystal Ag (111), Applied Physics Letters **103**, 251605 (2013).

[28] Z. Y. Al Balushi, K. Wang, R. K. Ghosh, R. A. Vilá, S. M. Eichfeld, J. D. Caldwell, X. Qin, Y.-C. Lin, P. A. DeSario, G. Stone, *et al.*, Two-dimensional gallium nitride realized via graphene encapsulation, Nature Materials **15**, 1166 (2016).

[29] A. Akbari, M. Naseri, and J. Jalilian, Tuning the electronic and optical properties of XP (X= Al, Ga) monolayer semiconductors using biaxial strain effect: modified Becke-Johnson calculations, Chemical Physics Letters **691**, 181 (2018).

[30] L. G. Arellano, F. de Santiago, Á. Miranda, F. Salazar, A. Trejo, L. A. Pérez, and M. Cruz-Irisson, Hydrogen storage capacities of alkali and alkaline-earth metal atoms on SiC monolayer: A first-principles study, International Journal of Hydrogen Energy **46**, 20266 (2021).

[31] L. G. Arellano, F. De Santiago, Á. Miranda, I. J. Hernández-Hernández, L. A. Pérez, and M. Cruz-Irisson, Hydrogen storage on bidimensional GeC with transition metal adatoms, Materials Letters **300**, 130239 (2021).

[32] L. G. Arellano, F. De Santiago, Á. Miranda, L. A. Pérez, F. Salazar, A. Trejo, J. Nakamura, and M. Cruz-Irisson, Ab initio study of hydrogen storage on metal-decorated GeC monolayers, International Journal of Hydrogen Energy **46**, 29261 (2021).

[33] P. Kumar, S. Singh, S. Hashmi, and K.-H. Kim, Mxenes: Emerging 2D materials for hydrogen storage, Nano Energy **85**,

105989 (2021).
[34] R. Varunaa and P. Ravindran, Potential hydrogen storage materials from metal decorated 2D-C_2 N: an ab initio study, Physical Chemistry Chemical Physics **21**, 25311 (2019).
[35] N. Khossossi, Y. Benhouria, S. R. Naqvi, P. K. Panda, I. Essaoudi, A. Ainane, and R. Ahuja, Hydrogen storage characteristics of li and na decorated 2D boron phosphide, Sustainable Energy & Fuels **4**, 4538 (2020).
[36] P. Gao, Z. Liu, and F. Zhang, Computational evaluation of Li-doped g-C_2N monolayer as advanced hydrogen storage media, International Journal of Hydrogen Energy **47**, 3625 (2022).
[37] B. Li, H. Xu, Y. Ma, and S. Yang, Harnessing the unique properties of 2D materials for advanced lithium–sulfur batteries, Nanoscale Horizons **4**, 77 (2019).
[38] N. Khossossi, D. Singh, A. Ainane, and R. Ahuja, Recent progress of defect chemistry on 2D materials for advanced battery anodes, Chemistry–An Asian Journal **15**, 3390 (2020).
[39] R. Rojaee and R. Shahbazian-Yassar, Two-dimensional materials to address the lithium battery challenges, ACS Nano **14**, 2628 (2020).
[40] M. C. Lucking, W. Xie, D.-H. Choe, D. West, T.-M. Lu, and S. Zhang, Traditional semiconductors in the two-dimensional limit, Physical Review Letters **120**, 086101 (2018).
[41] L. Qin, Z.-H. Zhang, Z. Jiang, K. Fan, W.-H. Zhang, Q.-Y. Tang, H.-N. Xia, F. Meng, Q. Zhang, L. Gu, D. West, S. Zhang, and Y.-S. Fu, Realization of AlSb in the double-layer honeycomb structure: A robust class of two-dimensional material, ACS Nano **15**, 8184 (2021).
[42] T. Wieting and J. Verble, Interlayer bonding and the lattice vibrations of β-GaSe, Physical Review B **5**, 1473 (1972).
[43] R. H. Bube and E. L. Lind, Photoconductivity of gallium selenide crystals, Physical Review **115**, 1159 (1959).
[44] M. Pashley, Electron counting model and its application to island structures on molecular-beam epitaxy grown GaAs (001) and ZnSe (001), Physical Review B **40**, 10481 (1989).
[45] J. Nakamura, H. Konogi, and T. Osaka, Inhomogeneous charge transfer in an incommensurate system, Physical Review B **51**, 5433 (1995).
[46] J. Nakamura, H. Nakajima, and T. Osaka, Structural stability and its electronic origin of the GaAs(111)A-(2x2) surface, Applied Surface Science **121-122**, 249 (1997).
[47] A. Ohtake, J. Nakamura, T. Komura, T. Hanada, T. Yao, H. Kuramochi, and M. Ozeki, Surface structures of GaAs{111}A,B-(2x2), Physical Review B **64**, 045318 (2001).
[48] J. Song, H. Y. Song, Z. Wang, S. Lee, J.-Y. Hwang, S. Y. Lee, J. Lee, D. Kim, K. H. Lee, Y. Kim, *et al.*, Creation of two-dimensional layered Zintl phase by dimensional manipulation of crystal structure, Science Advances **5**, eaax0390 (2019).
[49] Z. Guan, W. Yang, H. Wang, H. Wang, and J. Li, Direct band gap and anisotropic transport of ZnSb monolayers tuned by hydrogenation and strain, RSC advances **12**, 2693 (2022).
[50] A. Bafekry, M. Yagmurcukardes, M. Shahrokhi, M. Ghergherehchi, D. Kim, and B. Mortazavi, Electro-optical and mechanical properties of Zinc antimonide (ZnSb) monolayer and bilayer: A first-principles study, Applied Surface Science **540**, 148289 (2021).
[51] L. Meng, Y. Zhang, and S. Ni, Prediction of staggered stacking 2D BeP semiconductor with unique anisotropic electronic properties, Journal of Physics: Condensed Matter **32**, 085301 (2020).
[52] Q. Yan, Z. Li, P. Zhou, and L. Sun, Nontrivial topological states in new two-dimensional CdAs, Journal of Physics: Condensed Matter **33**, 365701 (2021).
[53] L. Ghalouci, B. Benbahi, S. Hiadsi, B. Abidri, G. Vergoten, and F. Ghalouci, First principle investigation into hexagonal and cubic structures of Gallium Selenide, Computational Materials Science **67**, 73 (2013).
[54] X. Li, M.-W. Lin, A. A. Puretzky, J. C. Idrobo, C. Ma, M. Chi, M. Yoon, C. M. Rouleau, I. I. Kravchenko, D. B. Geohegan, and K. Xiao, Controlled vapor phase growth of single crystalline, two-dimensional GaSe crystals with high photoresponse, Scientific Reports **4**, 5497 (2014).
[55] H. Nitta, T. Yonezawa, A. Fleurence, Y. Yamada-Takamura, and T. Ozaki, First-principles study on the stability and electronic structure of monolayer GaSe with trigonal-antiprismatic structure, Physical Review B **102**, 235407 (2020).
[56] P. Hohenberg and W. Kohn, Inhomogeneous electron gas, Physical Review **136**, B864 (1964).
[57] G. Kresse and J. Furthmüller, Efficient iterative schemes for ab initio total-energy calculations using a plane-wave basis set, Physical Review B **54**, 11169 (1996).
[58] G. Kresse and J. Furthmüller, Efficiency of ab-initio total energy calculations for metals and semiconductors using a plane-wave basis set, Computational Materials Science **6**, 15 (1996).
[59] J. P. Perdew, K. Burke, and M. Ernzerhof, Generalized gradient approximation made simple, Physical Review Letters **77**, 3865 (1996).
[60] J. Heyd, G. E. Scuseria, and M. Ernzerhof, Hybrid functionals based on a screened coulomb potential, The Journal of Chemical Physics **118**, 8207 (2003).
[61] P. E. Blöchl, Projector augmented-wave method, Physical Review B **50**, 17953 (1994).
[62] G. Kresse and D. Joubert, From ultrasoft pseudopotentials to the projector augmented-wave method, Physical Review B **59**, 1758 (1999).
[63] J. Klimeš, D. R. Bowler, and A. Michaelides, Chemical accuracy for the van der Waals density functional, Journal of Physics: Condensed Matter **22**, 022201 (2009).
[64] A. Togo and I. Tanaka, First principles phonon calculations in materials science, Scr. Mater. **108**, 1 (2015).
[65] J. Nakamura, H. Konogi, H. Sato, and T. Osaka, s-character of MX4 (M=C, Si, Ge, X=F, Cl, Br, I) molecules, Journal of the Physical Society of Japan **66**, 1656 (1997).

[66] H. Cai, Y. Gu, Y.-C. Lin, Y. Yu, D. B. Geohegan, and K. Xiao, Synthesis and emerging properties of 2D layered III–VI metal chalcogenides, Applied Physics Reviews **6**, 041312 (2019).

[67] C. H. Lee, S. Krishnamoorthy, D. J. O'Hara, M. R. Brenner, J. M. Johnson, J. S. Jamison, R. C. Myers, R. K. Kawakami, J. Hwang, and S. Rajan, Molecular beam epitaxy of 2D-layered gallium selenide on GaN substrates, Journal of Applied Physics **121**, 094302 (2017).

[68] X. Li, M.-W. Lin, A. A. Puretzky, J. C. Idrobo, C. Ma, M. Chi, M. Yoon, C. M. Rouleau, I. I. Kravchenko, D. B. Geohegan, *et al.*, Controlled vapor phase growth of single crystalline, two-dimensional GaSe crystals with high photoresponse, Scientific reports **4**, 1 (2014).

[69] S. Demirci, N. Avazlı, E. Durgun, and S. Cahangirov, Structural and electronic properties of monolayer group III monochalcogenides, Physical Review B **95**, 115409 (2017).

[70] M. Yagmurcukardes, R. T. Senger, F. M. Peeters, and H. Sahin, Mechanical properties of monolayer GaS and GaSe crystals, Physical Review B **94**, 245407 (2016).

[71] A. D. Becke and K. E. Edgecombe, A simple measure of electron localization in atomic and molecular systems, The Journal of Chemical Physics **92**, 5397 (1990), https://doi.org/10.1063/1.458517.

[72] K. Koumpouras and J. A. Larsson, Distinguishing between chemical bonding and physical binding using electron localization function (ELF), Journal of Physics: Condensed Matter **32**, 315502 (2020).

[73] *Chemistry data booklet* (International Baccalaureate Organization, Geneva, Switzerland, 2016) p. 9.

[74] G. Meyer, B. Voigtländer, and N. M. Amer, Scanning tunneling microscopy of surfactant-mediated epitaxy of Ge on Si(111): strain relief mechanisms and growth kinetics, Surface Science **274**, L541 (1992).

[75] M. Horn-von Hoegen, F. K. LeGoues, M. Copel, M. C. Reuter, and R. M. Tromp, Defect self-annihilation in surfactant-mediated epitaxial growth, Physical Review Letters **67**, 1130 (1991).

[76] A. P. Schnyder, S. Ryu, A. Furusaki, and A. W. W. Ludwig, Classification of topological insulators and superconductors in three spatial dimensions, Phys. Rev. B **78**, 195125 (2008).

[77] K. Saito, J. Nakamura, and A. Natori, Ballistic thermal conductance of a graphene sheet, Physical Review B **76**, 115409 (2007).